Bulletin of TICMI
Vol. 27, No. 2, 2023, 81–94

Power Spectra of Radio Waves Scintillation in the High-Latitude Conductive Terrestrial Ionosphere

George Jandieri[1], Akira Ishimaru[2], Vladimir Gavrilenko*[3], Nino Mchedlishvili[4], Oleg Kharshiladze[5]

[1]*Department of Stochastic Analysis and Mathematical Simulation, Georgian Technical University, Kostava str. 77, 0160, Tbilisi, Georgia*
[2]*Department of Electrical Engineering, University of Washington, 98195 Ft-10 Seattle, WA, USA*
[3]*Department of Radiophysics, Lobachevsky State University, 630950 Nizhni Novgorod, Russia*
[4]*Department of Control System, Georgian Technical University, 0160, Tbilisi, Georgia*
[5]*Department of Physics, Tbilisi State University, 0179 Tbilisi, Georgia*
(*Received March 05, 2023; Revised October 25, 2023; Accepted October 31, 2023*)

Ionospheric scintillation effects are investigated in the high-latitude conductive collisional ionospheric magnetized (COCOIMA) plasma by calculating the statistical characteristics of multiply scattered radio waves (RW) applying the modified perturbation method. Polarization coefficients in the polar COCOIMA plasma are derived for the first time. Differential equation for a random phase is derived. The variance and the auto-correlation function are obtained for any auto-correlation function of electron density fluctuations considering diffraction effects. Statistical moments contain: complex refractive index, polarization coefficients of both extraordinary and ordinary waves; orientation of an external magnetic field, Pedersen, Halls and longitudinal conductivities, parameters of elongated plasmonic irregularities and the velocity of a plasma flow. The scintillation level of scattered radio waves (RW) in the COCOIMA plasma is computed for the first time using zeroth, 1 st and square root 2nd moments of the power spectra. Oscillations of the scintillation spectrum are caused by the Fresnel filtering effect. It is possible to solve the opposite problem - calculate the velocity of a plasma flow and restore a structure of small-scale inhomogeneities than the Fresnel radius. Numerical simulations are interpreted for 3D anisotropic Gaussian and power-law spectral functions including axial ratio and an inclination angle of prolate plasmonic structures using the IRI model.

Keywords: Conductivity, plasma, statistical moments, radio waves, scintillation level, spectral width.

AMS Subject Classification: 26A33, 42B20.

1. Introduction

Random variations in the received signal due to the ionospheric plasma turbulence can represent the most severe limitation to the satellite and navigation systems caused by spatial-temporal variations of the signal amplitude and phase. The structure and formation of the ionospheric plasmonic inhomogeneities cause fluctuations in the propagation characteristics of scattered RW, which should be taken into

* Corresponding author. Email: vgg@rf.unn.ru,

ISSN: 1512-0082 print

account when calculating statistical characteristics [1-4]. The ionospheric scintillation phenomenon is one of the most deleterious factors, at least up to a frequency of 6-7 GHz in communication systems using the earth-space path. It is apparent that high-latitude electron density irregularities are caused by different geophysical processes. Ionospheric conductivities play an important role in these phenomena.

In order to assess the problem of degradation caused by scintillation and to work out remedies for a user in the subauroral to polar latitudes, two types of data are essential, namely, signal statistics and the morphology of scintillations. The signal statistic describes the distribution of the amplitude of scintillation and the fade rate along with the morphology, aim to present the designer of the system with an evaluation of the problems associated with the propagation path that are likely to be encountered by an operational or a planned satellite link. It also helps to supply the designer with the characteristics of the fading patterns that deteriorate the information flow. Scintillations disturb useful information about permanently existing anisotropic elongated plasmonic structures and various parameters in the polar conductive collision ionospheric plasma.

The geomagnetic field has an influence on the refractive index and anisotropy of electron density irregularities (on the axial ratio and orientation angle of elongated plasmonic structures). Using the GNSS characteristics sheet-like elongated plasmonic structures have been revealed. The wavefront of the GNSS signal undergoes refraction or diffraction depending upon the spatial scales of irregularities compared to the first Fresnel scale. The geomagnetic field causes the birefringence - generation of the ordinary (O-) and extraordinary (E-) waves. Peculiarities of the statistical characteristics of scattered RW scattered in the collision magnetoplasma have been considered [5-8] using WKB (Wentzel-Kramers-Brillouin) method or complex geometrical optics approximation.

Investigation of the scintillation effects in the polar conductive ionosphere is of great interest. The signal generating from that satellite propagates through the ionosphere contains information about moving irregular plasmonic irregularities along the whole path. The evolution of the diffraction pattern in the phase of the signal, is caused by the motion and the temporal changes of both the radio source and the motion of the irregularities. Scintillation level is based on the 3D spectral auto- correlation function of a random phase, the drift velocity of a plasma flow, the axial ratio of elongated plasmonic structures, orientation of an external magnetic field and the diffraction effects. Small-scale inhomogeneities are field aligned in a high-latitude ionosphere causing phase and amplitude fluctuations. Coherent scatter radars give the information on the Doppler shift of a scattered signal and the speed of motion of elongated plasmonic structures. Scintillation contains the spatial spectrum of field-aligned ionospheric irregularities and the relative velocity of these irregularities.

Scintillation phenomena of the O- and E-waves in the collisionless turbulent magneto plasma for the Gaussian and power-law spectral functions of electron density fluctuations have been investigated in [9-13] considering the diffraction effects.

In this paper we have presented evidence that the statistics of RW intensity scintillations can be accurately modeled by the Gaussian spectral function which is in conjunction with the diffraction effects. The second-order statistical moments of scattered RW in a high-latitude conductive terrestrial ionosphere are computed in Section 3 by applying the WKB method using the complex refractive index, polarization coefficients of both O- and E-waves and all the above-mentioned anisotropy

parameters. Numerical simulations are carried out for the anisotropic Gaussian auto-correlation function of electron density fluctuations in Section 4 applying IRI model. Conclusions are made in Section 5.

2. Diffraction parameter in a homogeneous conductive ionosphere

Initial is the wave equation for the electric field

$$\left(\nabla_i \nabla_j - \Delta\delta_{ij} - k_0^2 \tilde{\varepsilon}_{ij}\right) E_j\left(\mathbf{r}\right) = 0 \tag{1}$$

where: $\tilde{\varepsilon}_{ij} = \varepsilon_{ij} - i4\pi\sigma_{ij}/k_0 c$, σ_{ij} is the conductivity tensor, $k_0 = 2\pi/\lambda$, λ is the radio wavelength, Δ is the Laplacian, δ_{ij} is the Kronecker symbol. The external magnetic field $\mathbf{H}_0$ in the polar ionosphere is directed along the Z-axis vertically upwards, the wavevector of a refractive RW is located in the main (YOZ) of the Cartesian coordinate system. The dielectric permittivity tensor for a high-latitude COCOIMA plasma is given by

$$\begin{aligned}
\tilde{\varepsilon}_{xx} &= \varepsilon_\perp - i\left(\tilde{\sigma}_\perp + sg\right), \\
\tilde{\varepsilon}_{xy} &= -\tilde{\varepsilon}_{yx} = \cos\theta\left[s\text{æ}\delta - i\left(\tilde{\sigma}_H + \text{æ}\right)\right], \\
\tilde{\varepsilon}_{yy} &= \left(\varepsilon_\perp + p_0 u \sin^2\theta\right) - i\left[\left(\tilde{\sigma}_\perp \cos^2\theta + \tilde{\sigma}_\parallel \sin^2\theta\right)\right. \\
&\quad \left. + s\left(g - p_0 u g_1 \sin^2\theta\right)\right], \\
\tilde{\varepsilon}_{zz} &= \left(\varepsilon_\perp + p_0 u \cos^2\theta\right) - i\left[\left(\tilde{\sigma}_\parallel \cos^2\theta + \tilde{\sigma}_\perp \sin^2\theta\right)\right. \\
&\quad \left. + s\left(g - p_0 u g_1 \cos^2\theta\right)\right]
\end{aligned} \tag{2}$$

where: $p_0 = v/\left(1-u\right)$, $g = p_0\left(1+u\right)/\left(1-u\right)$, $\delta = 2/\left(1-u\right)$, $g_1 = \left(3-u\right)/\left(1-u\right)$, $\text{æ} = p_0\sqrt{u}$, $v\left(\mathbf{r}\right) = \omega_p^2\left(\mathbf{r}\right)/\omega^2$ and $u = \left(eH_0/m_e c\omega\right)^2$ are nondimensional magneto-ionic parameters of the plasma, $\omega_p\left(\mathbf{r}\right) = \left[4\pi N_e\left(\mathbf{r}\right) e^2/m_e\right]^{1/2}$. An imposed magnetic field makes an angle θ with the wave vector $\mathbf{k}$, $\tilde{\sigma}_{ij} = 4\pi\sigma_{ij}/k_0 c$ [14]

$$\begin{aligned}
\sigma_\perp &= e^2 n_e\left[\frac{\nu_e}{m_e\left(\nu_e^2+\omega_e^2\right)} + \frac{\nu_i}{m_i\left(\nu_{in}^2+\omega_i^2\right)}\right] \\
\sigma_H &= e^2 n_e\left[\frac{\omega_e}{m_e\left(\nu_e^2+\omega_e^2\right)} + \frac{\omega_i}{m_i\left(\nu_{in}^2+\omega_i^2\right)}\right] \\
\sigma_\parallel &= e^2 n_e\left[\frac{1}{m_e\nu_e} + \frac{1}{m_i\nu_{in}}\right]
\end{aligned}$$

here: $\sigma_\perp$, σ_H and $\sigma_\parallel$ are Pedersen, Hall's and longitudinal (parallel to Z-axis) conductivities, respectively; $n_e\left(\mathbf{r}\right) = n_0 + n_1\left(\mathbf{r}\right)$ is the electron density containing constant mean (n_0) and fluctuating term $n_1\left(\mathbf{r}\right)$ which is a random function of the spatial coordinates; e and m_e are the charge and the mass of an electron, $\nu_e = \nu_{ei} + \nu_{en}$ is the collision frequency of electron-ion (ν_{ei}) and electron-neutral

particles (ν_{en})

$$\nu_{ei} = N\left[59 + 4.18\log\left(\frac{T_e^3}{N}\right)\right] \times 10^{-6} T_e^{-3/2}[\text{m.k.s}]$$

and $\nu_{en} = 5.4\times10^{-16} N_n T_e^{1/2}$ [m.k.s]; ω_e and ω_i are the cyclotron frequencies for the electron and ion. Solution of (1) we will seek as $E_j(\mathbf{r}) = E_{0j}\exp(ik_0 z + ik_\perp y + \varphi_1)$; the direction of an incident wave coincides with the Z axis; the second term describes the diffraction effects; Third term is a random function of the spatial coordinates.

If $\theta = 0^\circ$ i.e. $\mathbf{k} \parallel \mathbf{H}_0$ we obtain an algebraic equation for the diffraction parameter $\mu = k_\perp/k_0$

$$\tilde{\varepsilon}_{xx}\mu^4 + \left[(\tilde{\varepsilon}_{xx} + \tilde{\varepsilon}_{zz})(1 - \tilde{\varepsilon}_{xx}) - \tilde{\varepsilon}_{xy}^2\right]\mu^2 + \tilde{\varepsilon}_{zz}\left(\left[(1 - \tilde{\varepsilon}_{xx})^2 + \tilde{\varepsilon}_{xy}^2\right]\right) = 0$$

describing an attenuation of RW in a homogeneous conductive plasma. For RW with the frequency of 3 MHz at an altitude 260 km the dumping coefficient is equal to 0.06, phase velocity is 10^3 km/sec.

3. Second order statistical moments of scattered radio waves in a high-latitude cocoima ionospheric plasma

When a plane wave is incident at a small angle on a plane layer of the COCOIMA plasma we will assume, that electron density irregularities are smooth in a scale of wavelength, i.e., transversal and longitudinal correlation scales satisfy the following conditions $l_\perp$, $l_\parallel \gg \lambda$. Diffraction effects are essential if a distance L (thickness of a plasma slab) propagated RW in the COCOIMA plasma is great enough: $L \gg l$.

Using the 2D Fourier transformation, in a first approximation from (1) we obtain

$$\frac{\partial\psi}{\partial z} + \frac{i}{k_x G_{1,2} - 2k_0}\left[k_x(k_y + k_\perp)P_{1,2} + k_x k_y G_{1,2} - k_y(k_y + 2k_\perp)\right]\psi = -\frac{ik_0^2}{k_x G_{1,2} - 2k_0} \cdot \left(\varepsilon_{xx}^{(1)} + \varepsilon_{xy}^{(1)} P_{1,2}\right) n_1(\mathbf{r}) \tag{3}$$

here: $P_{1,2} = \langle E_y\rangle / \langle E_x\rangle$, $G_{1,2} = \langle E_z\rangle / \langle E_x\rangle$ are the polarization coefficients, indices 1 and 2 correspond to the O- and E- waves, respectively. The ensemble average is denoted by the angled brackets. Below indices in the polarization coefficients are omitted for brevity.

The complex refractive index of the polar COCOIMA plasma at $s \ll \varepsilon_{ij}$, $\tilde{\sigma}_{ij}$ is given in [15]. In this region the polarization coefficients of scattered RW can be

written as

$$P_{1,2} = \frac{\langle E_y \rangle}{\langle E_x \rangle} = P'_{1,2} - iP''_{1,2}\,,$$
$$G_{1,2} = \frac{\langle E_z \rangle}{\langle E_x \rangle} = -G'_{1,2} + iG''_{1,2} \tag{4}$$

where $P'_{1,2} = \frac{1}{T_3^2+T_4^2}\left(T_1T_3 - T_2T_4\right)$,

$$P''_{1,2} = \frac{1}{T_3^2 + T_4^2}\left(T_1T_4 + T_2T_3\right),$$
$$T_3 = \left(\tilde{N}_2^2 - \tilde{\sigma}_{\parallel}\right) g_3\,,$$
$$G'_{1,2} = T_5 + T_7P'_{1,2} - T_8P''_{1,2}\,,$$
$$G''_{1,2} = T_6 - T_7P''_{1,2} - T_8P'_{1,2}\,,$$
$$g_0 = \varepsilon_{\perp} + p_0u\cos^2\theta, \quad T_5 = \frac{1}{\Delta}g_2g_3, \quad T_1 = \sin\theta\cos\theta$$
$$\left[\left(p_0 - \tilde{N}_1^2\right)p_0u - \left(N_2^2 - \tilde{\sigma}_{\perp}\right)\left(\sigma_{\parallel} - \sigma_{\perp}\right) - \left(æ + \sigma_H\right)^2\right],$$
$$T_2 = \left[\left(p_0 - \tilde{N}_1^2\right)\left(\tilde{\sigma}_{\parallel} - \tilde{\sigma}_{\perp}\right) + p_0u\left(N_2^2 - \tilde{\sigma}_{\perp}\right)\right]\sin\theta\cos\theta$$
$$T_4 = \left[p_0\left(1-u\right) - \tilde{N}_1^2\right] g_3\,, \quad T_6 = \frac{1}{\Delta}g_0g_3,$$
$$\Delta = \left(\varepsilon_{\perp} + p_0u\cos^2\theta\right)^2 + g_2^2, \quad g_2 = \tilde{\sigma}_{\parallel}\cos^2\theta + \tilde{\sigma}_{\perp}\sin^2\theta$$
$$T_7 = \frac{1}{\Delta}\left[p_0ug_0 + g_2\left(\tilde{\sigma}_{\parallel} - \tilde{\sigma}_{\perp}\right)\right]\sin\theta\cos\theta$$
$$T_8 = \frac{1}{\Delta}\left[p_0ug_2 - g_0\left(\tilde{\sigma}_{\parallel} - \tilde{\sigma}_{\perp}\right)\right]\sin\theta\cos\theta$$
$$p_0 = v/\left(1-u\right), \quad g_3 = \left(æ + \tilde{\sigma}_H\right)\sin\theta$$

Let a plane RW be incident on a turbulent COCOIMA plasma containing a large number of irregularities and propagates along the Z direction in a rectangular coordinate system. If phase fluctuations substantially exceed the amplitude fluctuations, using a double Fourier transform and the boundary condition $\psi\left(k_x, k_y, L=0\right) = 0$ at $s \ll \varepsilon_{ij}$, $\tilde{\sigma}_{ij}$ from (3) we obtain

$$\psi\left(x,y,L\right) = \frac{k_0}{2}\left(C_1 + iC_0\right)\int_0^L dz' n_1\left(x,y,z'\right)$$
$$\exp\left[-\frac{1}{4}\left(d_0 + id_1\right)k_0\left(L - z'\right)\right] \tag{5}$$

where: $C_0 = p_0 + P''\left(æ + \tilde{\sigma}_H\right)\cos\theta$,

$$C_1 = \tilde{\sigma}_{\perp} + P'\left(+\tilde{\sigma}_H\right)\cos\theta$$

$$
\begin{aligned}
d_0 &= \left[2G'G'' - \left(G'P'' + G''P'\right)(y+\mu)\right]x^2 \\
&\quad \left[G''y^2 + 2\left(\mu G'' - P''\right)y - 2\left(G'' - \mu P''\right)\right]x \\
d_1 &= \left[\left(G'^2 + G''^2\right) - \left(G''P'' + G'P'\right)(y+\mu)\right]x^2 \\
&\quad + \left[G'y^2 + 2\left(\mu G' - P'\right)y - 2\left(P'\mu - G'\right)\right]x \\
&\quad + 2y\,(y+2\mu)
\end{aligned}
$$

$x = k_x/k_0$ and $y = k_y/k_0$ are nondimensional wave vector parameters.

For an arbitrary spectral function $V_n(\mathbf{k})$ of electron concentration fluctuations the variance of the phase fluctuations can be written as

$$
\left\langle \varphi_1^2 \right\rangle = \frac{\sigma_n^2}{16\pi^{1/2}} \frac{\xi^3 k_0 L}{\chi^2} \left[\left(C_0^2 - C_1^2\right) + 2iC_0C_1\right]
$$

$$
\int_{-\infty}^{\infty} dx \int_{-\infty}^{\infty} dy V_n \left[k_0 x, k_0 y, k_0 \left(\Phi_4 - i\Phi_3\right)\right] \tag{6}
$$

here:

$$
\begin{aligned}
\Phi_3 &= \left(G'P'' + G''P'\right)yx^2 + \left[-G''y + 2\left(G'' + \mu P''\right)\right]x\,, \\
\Phi_4 &= \left(G''P'' + G'P'\right)yx^2 + \left[-G'y + 2\left(P'\mu - G'\right)\right]x - 4\mu y
\end{aligned}
$$

The auto-correlation function is given by

$$
W_\varphi(\zeta_x, \zeta_y, L) \equiv \left\langle \varphi_1(\mathbf{r})\, \varphi_1^*(\mathbf{r} + \boldsymbol{\rho}) \right\rangle = \frac{\pi}{2} \xi^3 k_0 L \left(C_0^2 + C_1^2\right).
$$

$$
\int_{-\infty}^{\infty} dx \int_{-\infty}^{\infty} dy V_n \left(k_0 x, k_0 y, k_0 \Psi_0\right) \exp\left(-i\zeta_x x - i\zeta_y y\right) \tag{7}
$$

here:

$$
\begin{aligned}
\Psi_0 &= \left[\left(G'^2 + G''^2\right) - \left(G''P'' + G'P'\right)(y+\mu)\right]x^2 \\
&\quad + \left[G'y^2 + 2\left(\mu G' - P'\right)y - 2\left(P'\mu - G'\right)\right]x + 2\left(y^2 + 2\mu y\right)
\end{aligned}
$$

$\zeta_x = k_0\rho_x$, $\zeta_y = k_0\rho_y$, ρ_y and ρ_x are distances between observation points in the main and perpendicular planes, respectively; an asterisk indicates the complex conjugate.

Small-scale plasmonic structures (from hundreds of meters up to kilometers) mainly have an influence on the amplitude scintillation of radio signals, while the large-scale irregularities give a contribution to the phase fluctuations. The index S_4 describing the expected diffraction pattern on the ground is connected with the phase auto-correlation function.

The drift velocity V_x of "frozen-in" electron density irregularities is inversely proportional to the Fresnel radius $(\lambda L)^{1/2}$. The scintillation level S_4 (1st and square

root 2nd moments) describing the scintillation rate can be calculated using the power spectrums $P_s(\nu)$ [16]

$$S_4^2 = \int_0^\infty dv P_s(\nu) \ , \quad \nu_{1S} = \frac{4}{S_4^2} \int_0^\infty d\nu \nu P_s(\nu) \ ,$$

$$\nu_{2S} = \frac{2}{S_4} \left[\int_0^\infty d\nu \nu^2 P_s(\nu) \right]^{1/2} ,$$

$$P_\varphi(\nu, L) = \frac{2\pi}{V_x} \int_0^\infty dk_x V_\varphi \left(k_x = \frac{2\pi\nu}{V_x}, k_y, L \right)$$

$$P_S(\nu, L) = 4P_\varphi(\nu, L) \sin^2 \left(\frac{\nu}{\nu_f} \right)^2 \tag{8}$$

ν is the scintillation frequency. For weak scattering if rigid plasmonic irregularities are moving along the X direction (perpendicular to the main plane), the power spectrum is proportional to the phase spectrum $P_s(\nu) = 4P_\varphi(\nu)$, where $\nu_f = V_x / (\pi\lambda L)^{1/2}$ is the Fresnel frequency, $F(\nu) = 4\sin^2(\nu/\nu_f)^2$ is the Fresnel filtering factor. There is a coupling between the irregularities and a drift velocity. The sinusoidal term describes oscillations in the scintillation spectrum.

4. Numerical calculations

Currently the high-latitude ionosphere is of great interest. Phase scintillation is an experimentally observing parameter by receiving antennas or radar systems. Scintillation becomes essential if the Fresnel radius of a scattered RW is of the order of the linear scales of elongated ionospheric irregularities at different altitudes of the ionosphere. It depends on a magneto-ionic parameters, the velocity of a plasma flow, thickness of a plasma slab, parameters of anisotropic electron density irregularities, the frequency of an incident RW, orientation and activity of the geomagnetic field, local time and seasons.

It is well known that the frequency range of 0.08-1 Hz relates to the 1-st Fresnel zone of small-scale electron density inhomogeneities from hundred meters to several kilometers. The cross-field anisotropy, being more significant for phase scintillations, appears at the scales $l_\perp > 0.5$ km and increases up to $l_\perp > 5 \div 10$ km, where the N-S component of the power spectrum of the phase fluctuation tends to the saturation; at high latitudes generate "sheets" and "wings" with different inclination angles relatively geomagnetic field.

Geomagnetic field in a high-latitude COCOIMA plasma generates mainly field aligned vertically elongated electron density irregularities of different scales. The transverse characteristic linear scales (relative to the geomagnetic field direction) of these plasmonic structures vary in the interval $1 \leq l_\perp \leq 10$ m up to $0.5 < l_\perp < 5 \div 10$ km playing an important role in the phase fluctuations. Observations show [17-21]

that in summer these inhomogeneities represent horizontally stratified structures and are transformed into plume structures in the equinox. In the height range $150 \div 257$ km small-scale electron density irregularities with the linear scales of few hundred meters are also observed in this region. Small-scale plasmonic structures are mainly aligned with an external magnetic field, but sometime inclination angle varies in the interval. $10^{\circ} \div 20^{\circ}$. Spectral functions of similar irregularities can be described analytically by power-law and anisotropic Gaussian spectral functions. The IRI model [22,23] is applied for the investigation of RW propagation in the polar ionosphere.

One important problem is the spatial spectral function at different altitudes. In numerical simulations we adopt a 3D anisotropic Gaussian spectral function [8]. Incident RW with a frequency of 3 MHz ($k_0 = 6.28 \cdot 10^{-2} \mathrm{m}^{-1}$) propagates along Z-axis. A numerical simulation is described by the anisotropic power-law and Gaussian spectral functions [15,24,25]

$$V_n(\mathbf{k}) = \frac{\sigma_n^2}{8\pi^{5/2}} \frac{A_p l_{\parallel}^3}{\chi^2 \left[1 + l_{\perp}^2 \left(k_x^2 + k_y^2\right) + l_{\perp}^2 k_z^2\right]^{p/2}}$$

$$\exp\left(-\frac{k_x^2 l_{\perp}^2}{4} - p_1 \frac{k_y^2 l_{\parallel}^2}{4} - p_2 \frac{k_z^2 l_{\parallel}^2}{4} - p_3 k_y k_z l_{\parallel}^2\right)$$

$$V_n(\mathbf{k}) = \frac{\sigma_n^2}{8\pi^{3/2}} \frac{l_{\parallel}^3}{\chi^2} \exp\left(-\frac{k_x^2 l_{\perp}^2}{4} - p_1 \frac{k_y^2 l_{\parallel}^2}{4} - p_2 \frac{k_z^2 l_{\parallel}^2}{4} - p_3 k_y k_z l_{\parallel}^2\right) \tag{9}$$

where: $p_1 = \left(\sin^2\gamma_0 + \chi^2 \cos^2\gamma_0\right)^{-1} \left[1 + \left(\chi^2 - 1\right)^2\right.$

$$\left. \cdot \sin^2\gamma_0 \cos^2\gamma_0 / \chi^2\right], \quad p_2 = \left(\sin^2\gamma_0 + \chi^2 \cos^2\gamma_0\right) / \chi^2,$$

$p_3 = \left(\chi^2 - 1\right) \sin\gamma_0 \cos\gamma_0 / 2\chi^2$, σ_n^2 is the variance of electron density fluctuations, $\chi = l_{\parallel}/l_{\perp}$ is the ratio of characteristic linear scales of electron density irregularities in a field aligned and transverse directions, γ_0 is the orientation angle of prolate plasmonic structures relative to the ambient geomagnetic field, is the spectral index, $A_p = \Gamma(p/2)$.

$$\Gamma\left[(5-p)/2\right] \sin\left[(p-3)\pi/2\right]$$

The Gadanki MST radar observations show that elongated plasmonic structures with linear scales between a few centimeters to a few hundreds of kilometers are exited [21,26] due to the Rayleigh-Taylor instability. In equinox, they have plume structures, in summer - horizontally stratified structures. Below 350 km velocity of plasmonic structures drifting normal to the geomagnetic field is of the order 10-100 m_S^{-1} and sometimes reaches 300 m_S^{-1}.

Numerical simulations are carried out using the IRI model [21,22]. The variance of the phase (6) for the Gaussian spectral function (9) has the following form:

$$\left\langle \varphi_1^2 \right\rangle = \frac{\sigma_n^2}{16\sqrt{\pi}} k_0 L \frac{\xi^3}{\chi^2} \left[\left(C_0^2 - C_1^2 \right) + 2iC_0C_1 \right]$$

$$\int_{-\infty}^{\infty} dx \int_{-\infty}^{\infty} dy \exp\left[-\frac{\xi^2}{4} \left(\Lambda_1 - i\Lambda_2 \right) \right] \tag{10}$$

where: $\Lambda_1 = \frac{1}{\chi^2} x^2 + p_1 y^2 + p_1 \left(\Phi_4^2 - \Phi_3^2 \right) + 4p_3 y \Phi_4$,
$\Lambda_2 = 2\Phi_3 \left(p_2 \Phi_4 + 2y \right)$.
Second order statistical moments of the phase fluctuations may be written as

$$W_\varphi \left(\zeta_x, \zeta_y, L \right) = \frac{\sigma_n^2}{16\sqrt{\pi}} k_0 L \cdot \frac{\xi^3}{\chi^2} \left(C_0^2 + C_1^2 \right) \int_{-\infty}^{\infty} dx \int_{-\infty}^{\infty} dy$$

$$\exp\left\{ -\frac{\xi^2}{4} \left[\psi_1 x^4 + \psi_2 x^3 + \left(\psi_3 + \frac{1}{4\chi^2} \right) x^2 + \psi_4 x + \left(p_1 y^2 + \psi_5 \right) \right] \right\} \tag{11}$$

where: $\psi_1 = p_2 e_0^2$, $\psi_2 = 2p_2 e_0 e_1$, $e_2 = 2\left(y^2 + 2\mu y \right)$

$$\begin{aligned}
\psi_3 &= p_2 e_1^2 + 2p_2 e_0 e_2 + 4p_3 y e_0 \,, \quad \psi_5 = e_2 \left(p_2 e_2 + p_3 y \right) \\
\psi_4 &= 2e_1 \left(p_2 e_2 + 2p_3 e_1 \right), \quad e_2 = 2\left(y^2 + 2\mu y \right), \\
e_0 &= \left(G'^2 + G''^2 \right) - \left(G'' P'' + G' P' \right) \left(y + \mu \right), \\
e_1 &= G' y^2 + 2\left(\mu G' - P' \right) y - 2\left(P' \mu - G' \right).
\end{aligned}$$

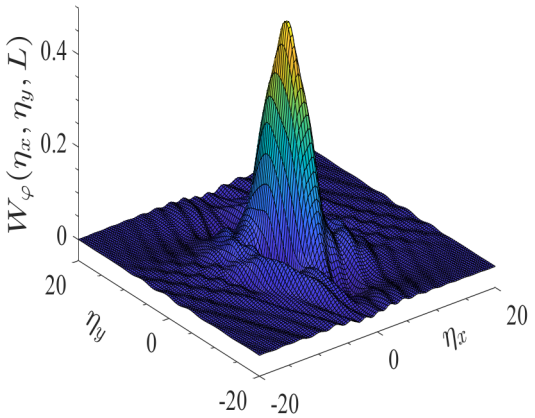

Figure 1. 3D auto-correlation function of the phase fluctuations.

The scintillation level is estimated for different anisotropy parameters χ and γ_0.

Figure 1 illustrates 3D correlation function of the phase fluctuations versus nondimensional distance parameters between the observation points in the main and perpendicular planes.

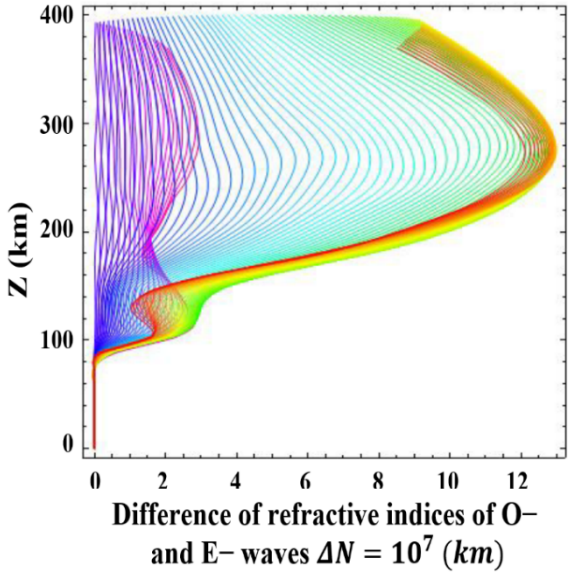

Figure 2. The dependence of the difference between refraction indices of the O- and E waves versus altitude

From Fig. 2 follows that the shapes of the curves correlate with the electron concentration profiles along the ray trajectories.

Figure 3 represents the scintillation level S_4 versus the variance of the normalized RMS deviation of electron density fluctuations σ_n at vertical sounding of RW ($\Theta = 0^\circ$) and different phase spectral index p. The error of the phase of the navigation radio signal radiating by the satellite contains the variance of a radio signal phase fluctuation, the variance of a thermal noise and the variance of a generator's noise. Ionospheric scintillations caused by phase fluctuations of the navigation radio signals are considered. The scintillation level S_4 is used to estimate the depth of ionospheric fading at the observation point. Three levels are distinguished on Fig. 3. At $S_4 < 0.3$ characterizes low-intensity scintillation; $0.3 \leq S_4 \leq 0.6$ - average intensity; $S_4 < 0.6$ – high intensity. Measurements show that at natural ionospheric perturbations, the typical value of the scintillation index for the equatorial regions is $S_4 \approx 0.3$ and sometimes it reaches $S_4 \approx 0.5 \div 0.8$. At high latitudes, the scintillation index is quite small and rarely exceeds $S_4 \approx 0.2$

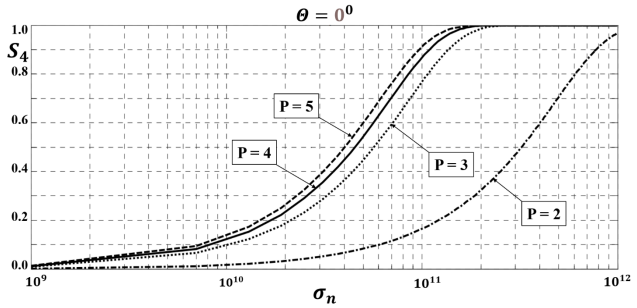

Figure 3. Scintillation level S_4 at vertical sounding of RW.

Figure 4 illustrates the normalized scintillation level $S_* = S_4/\sqrt{\langle\varphi_1^2\rangle}$ of scattered RW as a function of the parameter $\Upsilon = 2k_0^2/k_f^2$ based on the spectrum (9) if observation points are located at small distances. Left asymptotic area $\Upsilon \ll 1$ is devoted to the significant filtering, right area $\Upsilon \gg 1$ describes the fully developed diffraction area. In this region excitation of harmonic oscillations corresponds to the new waves propagating in the polar conductive terrestrial ionosphere. Second area connects these areas. In a Fig. 4a curve 1 describes the isotropic case ($\chi = 1$, $\gamma_0 = 0°$),curve 3 describes excitation of new wave in the terrestrial ionosphere due to conductivity ($\chi = 14$, $\gamma_0 = 15°$), curve 4 ($\chi = 20$, $\gamma_0 = 20°$) is the same as in a nonconductive ionosphere. Oscillations are at $\Upsilon = 25$ for field-aligned irregularities. In the case $\chi = 30$ and $\gamma_0 = 20°$ oscillations are stationary $\Upsilon = 38$. That is conductivity leads to the generation of new wave and/or geomagnetic Pc pulsations propagating in the ionosphere and/or in space. Figure 4b represents the normalized scintillation level S_* at $\xi = 80$ ($l_\parallel = 1.5$ km), $\zeta_x = 5$, $\zeta_y = 4$. Curve 3 does not oscillates in the area 2; four minimums arise in the fully-developed diffraction region. Curve 4 contains 15 minimums satisfying the condition: ...

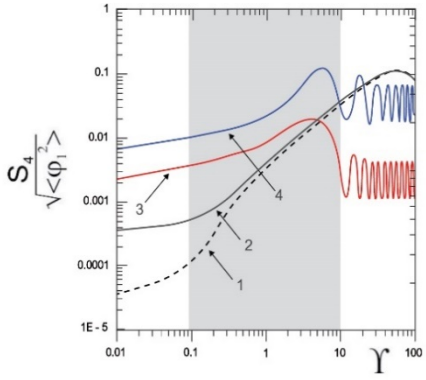

Figure 4a. The normalized scintillation level $S_* = S_4/\sqrt{\langle\varphi_1^2\rangle}$ versus parameter Υ at $\xi = 20$, observation points are located at $\zeta_x = 6$, $\zeta_y = 11$.

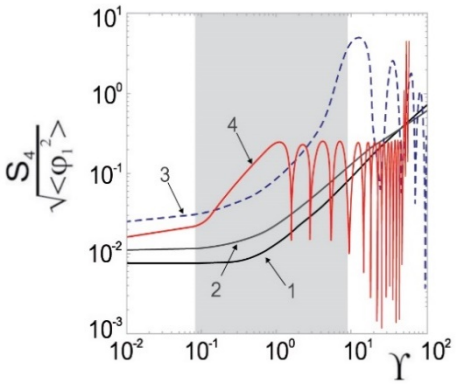

Figure 4b. The normalized scintillation level versus parameter Υ at $\xi = 10$, $\chi = 10 \div 30$, $\gamma_0 = 5° \div 20°$

Figure 5 shows the scintillation level versus anisotropy coefficient χ at parameters: $\mu = 0.06$, $\xi = 200$, $\Psi = \nu_0/\nu_f = 10$, $\nu_0 = k_0 V_x/2\pi$, $k_0 L = 0.1$, "frozen-in" elongated plasmonic structures are moving along the X-axis with a velocity of 100 m/sec at an incident 3 MHz RW. For a field aligned irregularities $\gamma_0 = 0°$ the spectral index

reaches $S_4 \approx 0.2$ for both waves at $\chi = 12$ (for the O-wave) and at $\chi = 19$ (for the E-wave); at $\gamma_0 = 10^\circ$ we have $S_4 = 0.1$ ($\chi = 12$ and $\chi = 19$ for O- E-waves, respectively); for $\gamma_0 = 30^\circ$: $S_4 = 0.05$ at $\chi = 12$ (for the O-waves) and $S_4 = 0.09$ at $\chi = 18$ (for the E-wave). Hence, the scintillation index decreases in proportion of the orientation angle and anisotropy coefficient of electron density irregularities.

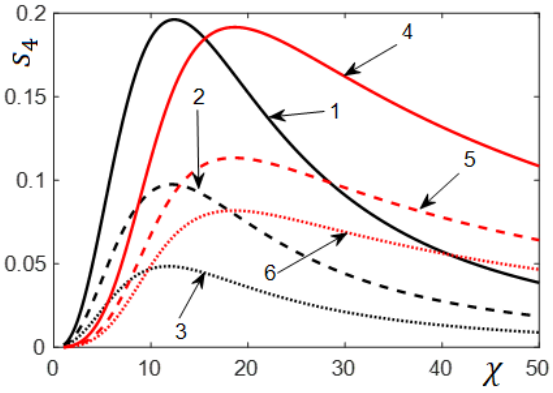

Figure 5. The relation between the scintillation level S_4 and the anisotropy factor χ at different inclination angle γ_0. Red color is devoted to the O-waves, black color – to the E-wave. Curves 1 and 4 are devoted to the angle $\gamma_0 = 0^\circ$; curves 2 and 5 correspond to $\gamma_0 = 10^\circ$ curves 3 and 6 – to the $\gamma_0 = 30^\circ$;

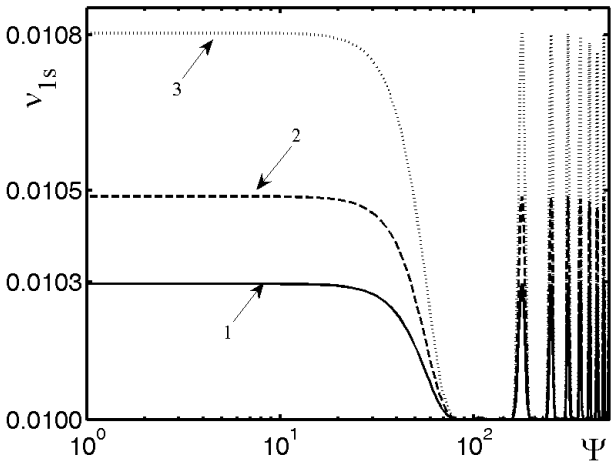

Figure 6. The width (1st moment) of the power spectrum.

Figure 6 describes the width (8) of the of the power spectrum (9). Curve 1 is devoted to the field-aligned elongated plasmonic structures ($\gamma_0 = 0^\circ$), curve 2 - $\gamma_0 = 20^\circ$, curve 3 – $\gamma_0 = 30^\circ$. Breaking parameters are at: $\Psi = 17$ (curve 1), $\Psi = 19$ (curve 2), $\Psi = 21$ (curve 3). The spectral width is of the order of $\nu_{2s} = 104$ mHz, while $\nu_{1S} \sim 10$ MhZ; If irregularities move along the Y axis with the same velocity, the width of the power spectrum increases up to $\nu_{2S} = 118$ mHz. Scintillation period is of the order of $T_{1S} \sim 80$ sec.

5. Conclusion

Second order statistical characteristics of a scattered RW are calculated and the scintillation effects in the polar COCOIMA plasma are considered for the first time applying the modified perturbation method taking into account: orientation of an external magnetic field, diffraction effects, polarization coefficients of both O- and E- waves, complex refractive index, anisotropy parameters of elongated plasmonic structures. In this region elongated plasmonic structures have different shapes due to the diffusion processes.

It was established that scintillation effects substantially depend on the ionospheric conductivities and the perturbation level of the ionosphere at different altitudes.

Log-log plots of the normalized scintillation level show that oscillations arise in a fully developed diffraction pattern (significant Fresnel filtering region). Excitation of new waves depends on the anisotropic parameters and a location of the observation points. First and second moments of the power spectrum are computed using the scintillation level.

The scintillation level decreases in proportion of the orientation angle and anisotropy factor of elongated plasmonic structures.

The obtained results will have great practical application in the satellite communications.

Acknowledgement

This research was funded by Shota Rustaveli National Science Foundation of Georgia (SRNSFG), grant NFR-21-316 "Investigation of the statistical characteristics of scattered electromagnetic waves in the terrestrial atmosphere and application".

References

[1] J. Aarons. *Global Morphology of Ionospheric Scintillation*. Proc. IEEE, **70** (1982), 360-378
[2] A. W. Wernik, J. A. Secan and E. J. Fremouw. *Ionospheric Irregularities and Scintillation*, Adv. Space Research, **31** (2003), 971-981
[3] S. Aol., S. Buchert, and E. Jurua. *Ionospheric Irregularities and Scintillations: a Direct Comparison of in Situ Density Observations with Ground-Based L-Band Receivers*, Earth, Planets and Space, **72** (2020), 2-15, Doi: 10.1186/s40623-020-01294-z
[4] A. Spicher, et all. *Interferometric Study of Ionospheric Plasma Irregularities in Regions of Phase Scintillations and HF Backscatter*, Geophys. Research Letters, **49** (2022), 1-11, Doi: 10.1029/2021GL097013
[5] A. Ishimaru, *Wave Propagation and Scattering in Random Media, Vol. 2, Multiple Scattering, Turbulence, Rough Surfaces and Remote Sensing,* IEEE Press: Piscataway, New Jersey, USA, 1997
[6] B. N. Gershman, L. M. Erukhimov, and Yu. A. Yashin. *Wavy Phenomena in the Ionosphere and Cosmic Plasma* (Russian), Nauka: Moscow, USSR, 1997
[7] Yu. A. Kravtsov, Yu. A Feizulin, and A.G. Vinogradov. *Wavy Phenomena in the Ionosphere and Cosmic Plasma* (Russian), Nauka: Moscow, USSR, 1997
[8] G. Jandieri, A. Ishimaru, V. Jandieri, A. Khantadze, and Zh. Diasamidze. *Model Computations of the Angular Power Spectra for Anisotropic Absorptive Turbulent Magnetized Plasma*, PIER, **70** (2007), 307-328, DOI: 10.2528/PIER070113103
[9] G. Jandieri, Zh. Diasamidze, and M. Diasamidze. *Scintillation Spectra of Scattered Electromagnetic Waves in the Turbulent Magnetized Plasma*, J. Basic and Applied Phys, **2** (2013), 224-234, ISSN: 2304-9332
[10] G. Jandieri, Zh. Diasamidze, and M. Diasamidze. *Scintillation effects and the Spatial Power Spectrum*, J. Adv. Physics, **13** (2017), 4593-4599, DOI: 10.24297/jap.v13i1.5638
[11] G. Jandieri, A. Ishimaru, B. Rawat, O. Kharshiladze, and Zh. Diasamidze. *Power spectra of ionospheric scintillations*, Advanced Electromagnetics, **6** (2017), 42-51, DOI: 10.7716/aem.v6i4.652
[12] G. Jandieri, A. Ishimaru, B. Rawat, V. Gavrilenko, and O. Kharshiladze. *Statistical Moments and Scintillation Level of Scattered Electromagnetic Waves in the Magnetized Plasma*, PIER C, **84** (2018), 11-22, DOI:10.2528/PIERC18030602

[13] P. Prikry, P.T. Jayachandran, R. Chadwick, and T. D. Kelly. *Climatology of GPS Phase Scintillation at Northern High Latitudes for the Period From 2008 to 2013*, Ann. Geophysics, **33** (2015), 531-545, DOI: 10.5194/angeo-33-531-2015

[14] V. L. Ginzburg. P*ropagation of electromagnetic waves in plasma. Gordon and Breach*, New York, USA, 1961

[15] G. Jandieri, A. Ishimaru, B. Rawat, and N. Tugushi. *Temporal Spectrum of a Scattered Electromagnetic Waves in the Conductive Collision Turbulent Magnetized Plasma*, Advanced Electromagnetics, **11** (2022), 1-8, 2022. DOI: 10.7716/aem.v11i1.1859

[16] C. L. Rufenach. *Ionospheric Scintillation by a Random Phase Screen: Spectralapproach*, Radio Science, **10** (1975), 155-165

[17] C.T. Nguyen, S. T. Oluwadare, N. T. Le, M. Alizadeh, J. Wickert, and H. Scuh. *Spatial and Temporal Distributions of Ionospheric Irregularities Derived from Regional and Global ROTI Maps*, Remote Sensing, **14** (2022), 1-25, DOI: 10.3390/rs14010010

[18] Y. Jin, Lasse, and et all. *Climatology and Modeling of Ionospheric Irregulaities Over Greenland Based on Empirical Orthogonal Function Method*, J. Space Weather Space Clim., **12** (2022), 2-16, DOI: 10.1051/swsc/2022022

[19] A. Spicher, and et all. *Interferometric Study of Ionospheric Plasma Irregulaities in Regions of Phase Scintillations and HF backscatter*, Geophysical Research Letters. **14** (2022), 1-25, DOI: 10.1029/2021GL097013

[20] C. T. Nguyen, S. T. Oluwadare, and et all. *Spatial and Temporal Distributions of Ionospheric Irregularities Derived from Regional and Global ROTI Maps*, Remote Sensing., **14** (2022), 1-25, DOI: 10.3390/rs14010010

[21] S. Raizada, S. S. Sinha. *Some New Features of Electron Density Irregularities Over SHAR During Strong Spread F.*, Ann. Geophys, **18** (2000), 141-151, DOI: 10.1007/s00585-000-0141-8

[22] D. Bilitza. *IRI the International Standard for the Ionosphere*, Adv. Radio Sci., **16** (2018), 1-11, DOI: 10.5194/ars-16-1-2018

[23] D. Bilitza, and et all., *The International Reference Ionosphere Model: A Review and Description of an Ionospheric Benchmark*, Reviews of Geophysics. **60** (2022), 1-65, DOI: 10.1029/2022RG000792

[24] G. Jandieri, and N. Tugushi. *Transformation of the Spatial Spectrum of Scattered Radio Waves in the Conductive Equatorial Ionosphere*, Electronics, **12** (2023), 2759-2770, DOI: 103390/electronics12132759

[25] G. Jandieri, and N. Tugushi. *Statistical characteristics of the temporal spectrum of scattered radiation in the equatorial ionosphere*, J. of Environmental & Earth Sciences., **5** (2023), 85-94, DOI: 10.30564/jees.v5il.5442

[26] K. Patra, and D. V. Phanikumar. I*ntriguing Aspects of F-region Plasma Irregularities Revealed by the Gadanki Radar Observations During the SAFAR Campaign*, Ann. Geophys, **27** (2009), 3781-3790, DOI: 10.5194/angeo-27-3781-2009